BULLETIN OF THE POLISH ACADEMY OF SCIENCES
TECHNICAL SCIENCES, Vol. 59, No. 4, 2011
DOI: 10.2478/v10175-011-0070-6

Efficiency improvement due to direct torque and flux three levels three areas control method applied to small hydroelectric power plant

K. KULIKOWSKI* and A. SIKORSKI

Division for Power Electronics and Electrical Drivers, Bialystok University of Technology, 45D Wiejska St., 15-351 Bialystok, Poland

Abstract. The paper presents a description of a new DTFC3L3A (direct torque and flux control three levels three areas) control method of induction machine as well as its comparison with the DTC method. The basis for the comparison is the switching frequency of described methods. The proposed method is optimized to reduce number of switchings (which is proportional to switching power losses) in static state, as well as it takes into account the δ angle which makes it possible to obtain a sinusoidal shape of flux within range of low angular frequencies of an asynchronous machine. The paper includes the results of experiments performed on a three level DC/AC inverter for both control methods.

Key words: asynchronous machine, AC/DC/AC converter, DC/AC converter, DTC, flux control.

1. Introduction

Most wind power stations, and even a greater number of hydropower plants are directly linked to electric grids. Generators in such plants work with constant angular velocity, which means that they can be exclusively used either at a considerable wind force or at high water level in a reservoir. However, the introduction of power electronics converters into the plants' power generation systems has made it possible to utilize weak winds or low water level in reservoirs as well eliminate some other operational disadvantages. But this additional module, despite being characterized by high efficiency (92–94%), has had, in the long run a negative impact on the efficiency of the whole device. In order to increase the converter's efficiency by a few percent, it is required to minimize the switching losses of the converter's switches as these losses often constitute more than 70% of the overall losses at the switching frequency of 20 kHz. Thus, the converter should by controlled in such way as to ensure the required parameters of the system such as torque or current pulsations at the lowest possible switching frequencies. The nonlinear control system considered in this paper is concerned with a three-level inverter cooperating with an asynchronous machine. Although, in the actual system the inverter cooperates with an asynchronous generator, the considerations presented in this paper are concerned with an asynchronous machine so that the authors' previous papers could be included.

The DTC method was proposed in the second half of the eighties by Takachashi and Noguchi [1]. Owing to its many advantages, the control method was very quickly introduced into industry and it is still being used for new applications [2]. Of course, the method has a few disadvantages but its numerous improvements and modifications [3-6] have considerably eliminated its shortcomings so that it has become competitive to field oriented control (FOC) methods [7–8]. Some of these modifications focus on the minimization of switching losses or torque ripple. The DTFC3A method [6–9] is an illustration of such a modification in which an optimum error distribution area has been introduced. The modification makes it possible to reduce switching frequency. The idea of optimum error distribution area extended to a three-level inverter capability is used in the DTFC-3L-3A method proposed here. The DTFC-3L-3A method is similar to the DPC-3L-3A (direct power control three levels three areas) [10] control method of AC/DC converters.

1.1. Mathematical model of an inverter.

The relationships (1) and (2) [9] describe the output voltage vectors of the inverter in $\alpha\beta$ stationary reference frame with respect to three- and two-level configurations (Fig. 1).

$$\boldsymbol{U}_d[n] = \begin{cases} \frac{2}{3}U_{dc} \cdot e^{j(n-21)\frac{\pi}{3}}, \text{ for } n = \{21, 22, ..., 26\}, \\ \frac{\sqrt{3}}{3}U_{dc} \cdot e^{j(n-15)\frac{\pi}{3}}, \text{ for } n = \{15, 16, ..., 20\} \\ \frac{1}{3}U_{dc} \cdot e^{j(n-3)\frac{\pi}{3}}, \text{ for } n = \{3, 4, ..., 14\} \\ \text{“0”}, \text{ for } n = \{0, 1, 2\} \end{cases}, \quad (1)$$

$$\boldsymbol{U}_d[n] = \begin{cases} \frac{2}{3}U_{dc} \cdot e^{j(n-1)\frac{\pi}{3}}, \text{ for } n = \{1, 2, ..., 6\}, \\ \text{“0”}, \text{ for } n = \{0, 7\} \end{cases} \quad (2)$$

where $\boldsymbol{U}_d\,[n]$ – inverter voltage vector, U_{dc} – DC link voltage, n – vector number (Fig. 1), "0" – zero vector.

*e-mail: k.kulikowski@pb.edu.pl

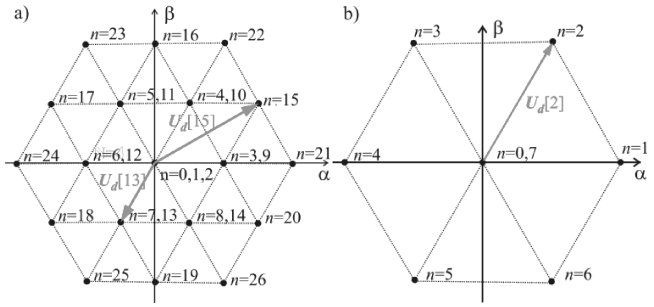

Fig. 1. Graphic representation of inverter voltage vectors in $\alpha\beta$ reference frame for three- (a) and two-levels (b) inverters

1.2. Mathematical model of an induction machine supplied by an inverter. An induction motor supplied by an inverter (Fig. 2) in a *dq* rotating reference frame can be described by formulas (3) and (3a) [9, 11].

$$\boldsymbol{U}_s[n] = R_s\boldsymbol{I}_s + j\omega_s L_{\sigma s}\boldsymbol{I}_s + L_{\sigma s}\frac{d}{dt}\boldsymbol{I}_s + j\boldsymbol{E} \tag{3}$$

$$\boldsymbol{U}_s[n] = \boldsymbol{U}_d[n]\cdot e^{-j\omega_s t}, \tag{3a}$$

where $\boldsymbol{U}_s\,[n]$ – inverter voltage vector in *dq* reference frame, $\boldsymbol{I}_s$ – stator current vector, $\boldsymbol{E}$ – vector of electromotive force, ω_s – angular speed of stator flux vector, R_s – stator resistance, $L_{\sigma s}$ – leakage inductance of windings.

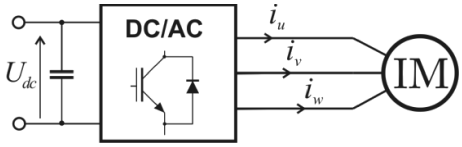

Fig. 2. Schematic diagram of induction machine supplied by an inverter

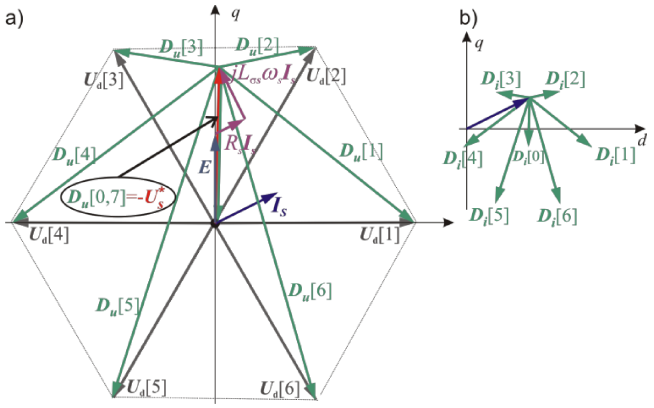

Fig. 3. Voltage vectors proportional to the vectors of current derivative $\boldsymbol{D}_u[n]$ (a), and corresponding vectors of current derivative $\boldsymbol{D}_i\,[n]$ (b)

Dependence (4) is described by transformation (3). The obtained voltage vector (Fig. 3a) is proportional to the vector of stator current derivative (5) (Fig. 3b) which determine both the direction and speed of current changes.

$$\begin{aligned}\boldsymbol{D}_i[n] &= \frac{d}{dt}\boldsymbol{I}_s = \\ &= \frac{1}{L_{\sigma s}}(-(R_s\boldsymbol{I}_s + j\omega_s L_{\sigma s}\boldsymbol{I}_s + j\boldsymbol{E}) + \boldsymbol{U}_s[n]),\end{aligned} \tag{4}$$

$$\mathbf{D}_u[n] = -\mathbf{U}_s^* + \mathbf{U}_s[n] \tag{4a}$$

$$\boldsymbol{D}_i[n] = \frac{1}{L_{\sigma s}}\boldsymbol{D}_u[n]. \tag{5}$$

2. Description of control methods

2.1. DTC. The DTC method (Fig. 4) makes it possible to control torque and flux by selecting inverter voltage vector $U_d\,[n]$ from the voltage vector selection table (Table 1). The choice depends on sector N as well as current states of the comparators. The selection of sector N is determined by the angle of flux vector. The states of the comparators are determined by the comparison results of the set and estimated values of torque and flux.

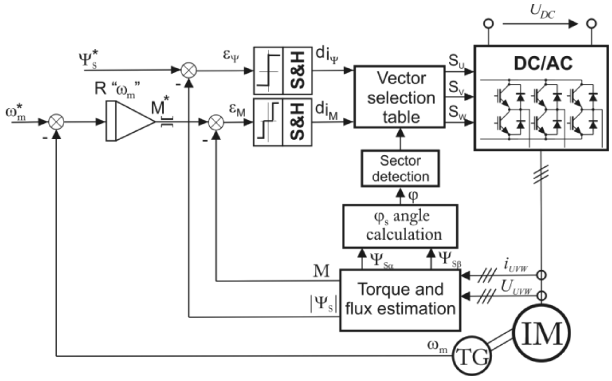

Fig. 4. Schematic diagram of DTC method

Table 1
Switching tabl for DTC method

		$N=1$	$N=2$	$N=3$	$N=4$	$N=5$	$N=6$
$d\Psi=1$	$dM=1$	$\boldsymbol{U}_d[2]$	$\boldsymbol{U}_d[3]$	$\boldsymbol{U}_d[4]$	$\boldsymbol{U}_d[5]$	$\boldsymbol{U}_d[6]$	$\boldsymbol{U}_d[1]$
	$dM=0$	$\boldsymbol{U}_d[7]$	$\boldsymbol{U}_d[0]$	$\boldsymbol{U}_d[7]$	$\boldsymbol{U}_d[0]$	$\boldsymbol{U}_d[7]$	$\boldsymbol{U}_d[0]$
	$dM=-1$	$\boldsymbol{U}_d[6]$	$\boldsymbol{U}_d[1]$	$\boldsymbol{U}_d[2]$	$\boldsymbol{U}_d[3]$	$\boldsymbol{U}_d[4]$	$\boldsymbol{U}_d[5]$
$d\Psi=0$	$dM=1$	$\boldsymbol{U}_d[3]$	$\boldsymbol{U}_d[4]$	$\boldsymbol{U}_d[5]$	$\boldsymbol{U}_d[6]$	$\boldsymbol{U}_d[1]$	$\boldsymbol{U}_d[2]$
	$dM=0$	$\boldsymbol{U}_d[0]$	$\boldsymbol{U}_d[7]$	$\boldsymbol{U}_d[0]$	$\boldsymbol{U}_d[7]$	$\boldsymbol{U}_d[0]$	$\boldsymbol{U}_d[7]$
	$dM=-1$	$\boldsymbol{U}_d[5]$	$\boldsymbol{U}_d[6]$	$\boldsymbol{U}_d[1]$	$\boldsymbol{U}_d[2]$	$\boldsymbol{U}_d[3]$	$\boldsymbol{U}_d[4]$

As shown in Fig. 5 [9], the division of the error area in the DTC method is not optimal. The determination of the optimal boundary requires a delimitation of such a dividing line where the impacts of the two adjacent voltage vectors are equivalent.

In order to analyze the influence of the vectors of current derivatives on the changes of torque and flux values, the errors of flux and torque should first be converted to the current scale and next they could be treated as current vector components (6) [6].

$$\boldsymbol{\varepsilon} = \varepsilon_d + j\varepsilon_q = c_\Psi\cdot\varepsilon_\Psi + jc_M\cdot\varepsilon_M, \tag{6}$$

$$c_\Psi = \frac{i_{sdN}}{\Psi_{sN}} = \frac{1}{L_m}, \tag{6a}$$

$$c_M = \frac{i_{sqN}}{M_N} \cong \frac{2\omega_{sN}}{3p_b U_N\sqrt{2}}, \tag{6b}$$

where c_Ψ, c_M – current scale factors with respect to flux and torque, Ψ_{sN} – nominal value of flux, i_{sqN}, i_{sdN} – nominal

value of stator current vector components, M_N – nominal value of torque, ω_{sN} – nominal value of synchronous angular speed, p_b – number of magnetic pole pair, U_n – nominal value of stator voltage.

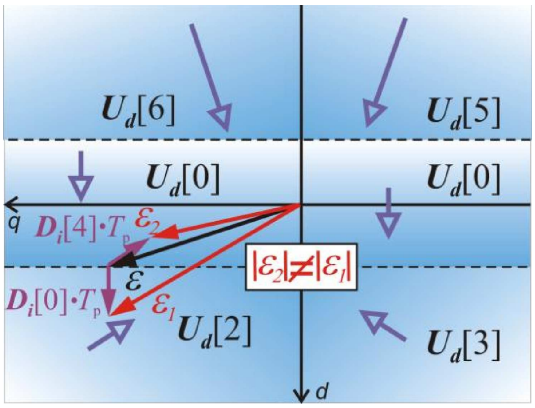

Fig. 5. Graphic representation of the division of the error area in the DTC method

2.2. The DTFC-3L-3A method. The DTFC-3L-3A method is a modification of DTFC-3A method making use of an increased number of active vectors of three – level inverter.

Using inverter voltage vectors that cause short current derivatives to reduce switching frequency in static state is desirable. It was shown in [9] that the above voltage vectors in the two-level inverter form an equilateral triangle (Fig. 6a) in each N sector, whereas in the three-level inverter each N sector can be divided into four similar deltas (Fig. 6b). Optimal error areas (Fig. 7) for each of the equilateral triangles can be determined in an analogous way to DTFC-3A method.

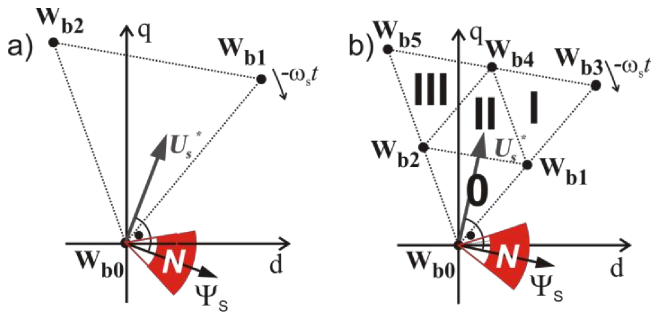

Fig. 6. Inverter voltage vectors made up of equilateral triangles in two- (DTFC-3A)(a) and tree-level (DTFC-3L-3A) (b) inverters

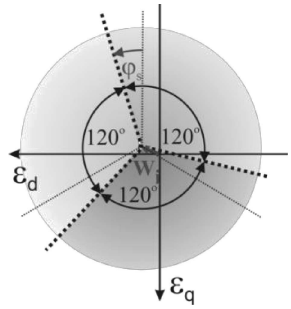

Fig. 7. Graphic representation of optimum error distribution area

It was shown [9] that the boundaries of a optimum error distribution area are made up of three half-lines of common origin, and turned against each other by 120°. These boundaries are shifted by angle φ_S with respect to the qaxis and the common origin of the boundaries is shifted from the origin of the coordinate system by $\boldsymbol{W}_i$ vector (Fig. 7).

$\boldsymbol{W}_i$ vector (7) is proportional to voltage vector $\boldsymbol{W}$ (8) that constitutes the difference between the $\boldsymbol{S}_t$ vector (centre of delta composed of three voltage vectors) and voltage vector $\boldsymbol{U}_p$ (Fig. 10). Vector $\boldsymbol{S}_t$ is dependent on the delta where the voltage vector $\boldsymbol{U}_s^*$ is currently located. The vector is described by formula (9).

$$\boldsymbol{W}_i = \frac{\boldsymbol{W}}{L_{\sigma s}} T_p, \tag{7}$$

where T_p – sampling time.

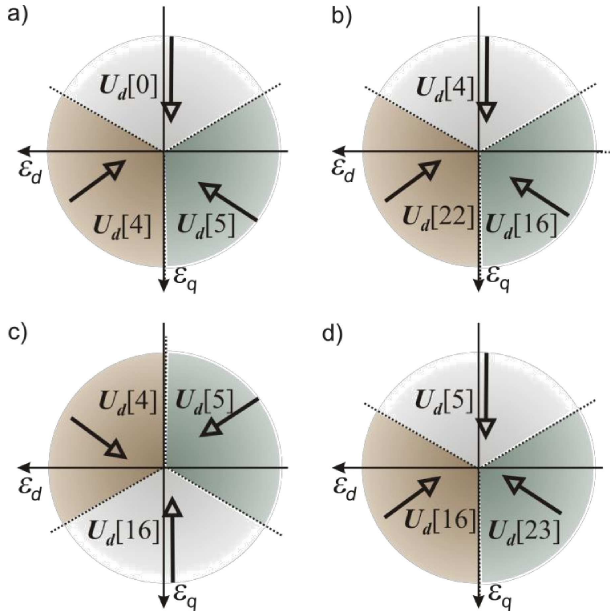

Fig. 8. Error distribution areas for triangles 0 (a), I (b), II (c) and III (d) in $N = 1$ sector

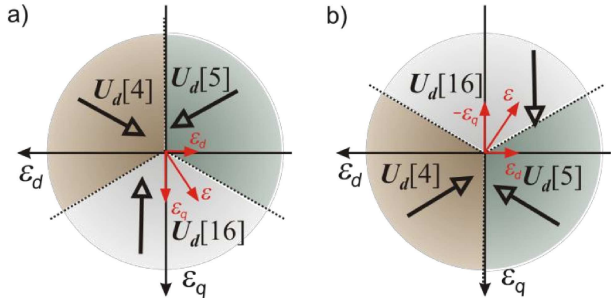

Fig. 9. Error distribution area in triangle II before (a) and after (b) the change of the sign of component q of the error vector in sector $N = 1$

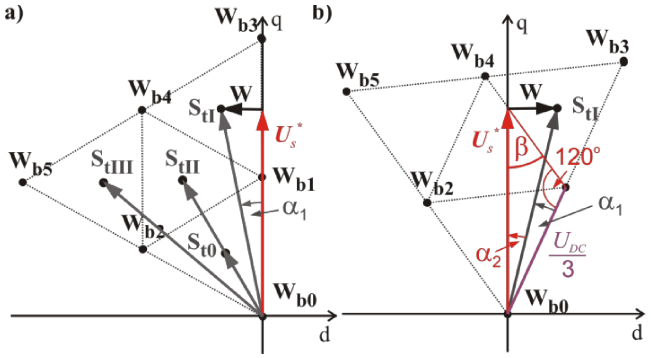

Fig. 10. Graphic interpretation of vector $\boldsymbol{W}$ in DTFC-3L-3A control method for both situations (when $\boldsymbol{U}_s^*$ vector is in the beginning (a) and in the end (b) of triangle I)

$\boldsymbol{W}$ vector is calculated using formula (8) as shown in Fig. 9.

$$\boldsymbol{W} = \boldsymbol{S}_t - \boldsymbol{U}_s^* \tag{8}$$

$$\boldsymbol{S_t} = \begin{cases} \frac{1}{3}(\boldsymbol{W}_{b0} + \boldsymbol{W}_{b1} + \mathbf{W}_{b2}), \text{ for triangle 0} \\ \frac{1}{3}(\boldsymbol{W}_{b1} + \boldsymbol{W}_{b3} + \mathbf{W}_{b4}), \text{ for triangle I} \\ \frac{1}{3}(\boldsymbol{W}_{b1} + \boldsymbol{W}_{b2} + \mathbf{W}_{b4}), \text{ for triangle II} \\ \frac{1}{3}(\boldsymbol{W}_{b2} + \boldsymbol{W}_{b4} + \mathbf{W}_{b5}), \text{ for triangle III} \end{cases} \tag{9}$$

where $\boldsymbol{W}_{b0}$, $\boldsymbol{W}_{b1}$, $\boldsymbol{W}_{b2}$, $\boldsymbol{W}_{b3}$, $\boldsymbol{W}_{b4}$, $\boldsymbol{W}_{b5}$ – currently used voltage vectors $\boldsymbol{U}_d$ [n] (Fig. 10).

In order to simplify the inverter control, vector $\boldsymbol{S}_t$ can be replaced by vector $\boldsymbol{S}$ (10), which is time independent. Vector $\boldsymbol{S}$ is averaging value of vector $\boldsymbol{S}_t$ in each of the triangles (Fig. 9).

$$\boldsymbol{S} = |\boldsymbol{S}|\, e^{j\varphi_S} =$$

$$= \begin{cases} \frac{2}{3}U_{DC} j\frac{\sqrt{2}}{4} e^{j\delta}, \text{ for triangle 0} \\ \frac{2}{3}U_{DC}\sqrt{\frac{7}{12}} e^{j\left(\frac{\alpha_1-\alpha_2}{2}+\frac{\pi}{2}+\delta\right)}, \text{ for triangle I} \\ \frac{2}{3}U_{DC} j\frac{\sqrt{2}}{2} e^{j\delta}, \text{ for triangle II} \\ \frac{2}{3}U_{DC}\sqrt{\frac{7}{12}} e^{j\left(\frac{\alpha_2-\alpha_1}{2}+\frac{\pi}{2}+\delta\right)}, \text{ for triangle III} \end{cases} \tag{10}$$

$$\alpha_1 = \operatorname{arctg}\left(\sqrt{3}/9\right), \tag{10a}$$

$$\alpha_2 = \frac{\pi}{3} - \beta - \alpha_1 = \frac{\pi}{3} - \arcsin\left(\frac{U_{DC}\sqrt{3}}{6\cdot|\boldsymbol{U}_s^*|}\right) - \alpha_1 \tag{10b}$$

$$\delta = \operatorname{arctg}\frac{-\mathrm{Re}(\boldsymbol{U}_s^*)}{\mathrm{Im}(\boldsymbol{U}_s^*)}, \tag{10c}$$

$$\boldsymbol{W} = \boldsymbol{S} - \boldsymbol{U}_s^*. \tag{10d}$$

Vector $\boldsymbol{U}_{sec1}$ and angle φ_{Usec2} (Fig. 11) are introduced in order to choose a suitable triangle. These variables are defined by Eqs. (12) and (13).

$$\boldsymbol{U}_{\mathrm{sec}\,1} = \boldsymbol{W}_{b4} = |\boldsymbol{U}_{\mathrm{sec}\,1}|\cdot e^{j\varphi_{\boldsymbol{U}_{\mathrm{sec}\,1}}}, \tag{12}$$

$$\varphi_{U_{\mathrm{sec}\,2}} = \arcsin\left(\frac{|\mathbf{U}_s|}{|\boldsymbol{U}_{\mathrm{sec}\,1} - \boldsymbol{U}_s|}\sin\left(\varphi_{U_{sec1}} - \varphi_{U_s}\right)\right). \tag{13}$$

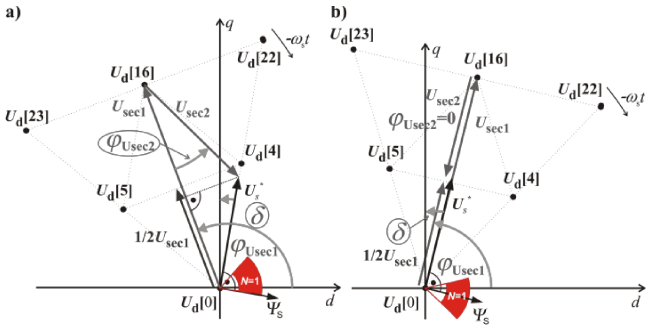

Fig. 11. Graphic interpretation of voltage vectors $\boldsymbol{U}_{sec1}$, and $\boldsymbol{U}_{sec2}$, as well as angle φ_{Usec2} for both situations (when flux vector is in the beginning (a) and in the middle (b) of sector N)

If the projection of vector $\boldsymbol{U}_s^*$ on $\boldsymbol{U}_{sec1}$ is shorter than half of vector's $\boldsymbol{U}_{sec1}$ length, then $\boldsymbol{U}_s$ [n] vector is located inside triangle 0. This condition is described by inequality (14).

$$\left|\frac{\boldsymbol{U}_{\mathrm{sec}\,1}}{2}\right| > \mathrm{Re}\left\{|\boldsymbol{U}_s|\, e^{j(\varphi_{U_{sec1}} - \varphi_{U_s})}\right\}. \tag{14}$$

In the case when inequality (12) is unfulfilled, the choice of triangle is dependent on φ_{Usec2} angle, according to Table 2.

Table 2
Triangle selection table

$\varphi_{U\,\mathrm{sec}\,2} \in (\pi/6, \pi/2)$	triangle I
$\varphi_{U\,\mathrm{sec}\,2} \in (-\pi/6, \pi/6)$	triangle II
$\varphi_{U\,\mathrm{sec}\,2} \in (-\pi/2, -\pi/6)$	triangle III

Ultimately, DTFC3L-3A control system for the three-level inverter takes the form shown in Fig. 12.

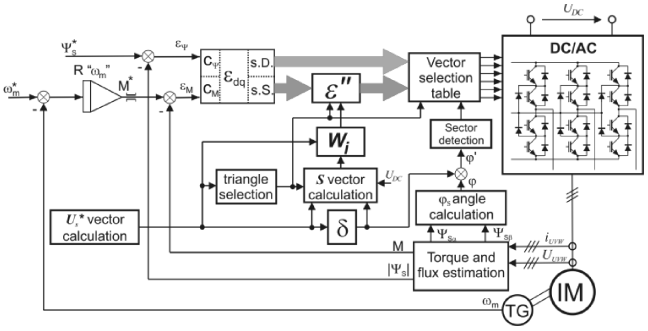

Fig. 12. Schematic diagram of DTFC-3L-3A method

In DTFC-3L-3A control method the real values of torque and flux are compared to corresponding set values. The obtained errors are computed to current scale in order to create current error vector ε (6). Error vector ε is thus subsequently transformed into ε'' in agreement with formula (15).

$$|\boldsymbol{\varepsilon}''|\cdot e^{j\varphi_{\varepsilon''}} =$$

$$= \begin{cases} (\varepsilon_d + j\varepsilon_q - \boldsymbol{W}_i)\cdot e^{-j\varphi_S}, \text{ for triangles 0,I,III} \\ (\varepsilon_d - j\varepsilon_q - \boldsymbol{W}_i)\cdot e^{-j\varphi_S}, \text{ for triangle II} \end{cases}. \tag{15}$$

Table 3
Vector selection table for DTFC3L3A

		$N=1$	$N=2$	$N=3$	$N=4$	$N=5$	$N=6$
$\varphi_{\varepsilon''}$	Triangle	inverter voltage vectors					
$\left(\frac{-\pi}{6},\frac{\pi}{2}\right)$	0	$\boldsymbol{U}_d$[4] $\boldsymbol{U}_d$[10]	$\boldsymbol{U}_d$[5] $\boldsymbol{U}_d$[11]	$\boldsymbol{U}_d$[6] $\boldsymbol{U}_d$[12]	$\boldsymbol{U}_d$[7] $\boldsymbol{U}_d$[13]	$\boldsymbol{U}_d$[8] $\boldsymbol{U}_d$[14]	$\boldsymbol{U}_d$[3] $\boldsymbol{U}_d$[15]
	I	$\boldsymbol{U}_d$[22]	$\boldsymbol{U}_d$[23]	$\boldsymbol{U}_d$[24]	$\boldsymbol{U}_d$[25]	$\boldsymbol{U}_d$[26]	$\boldsymbol{U}_d$[21]
	II	$\boldsymbol{U}_d$[4] $\boldsymbol{U}_d$[10]	$\boldsymbol{U}_d$[5] $\boldsymbol{U}_d$[11]	$\boldsymbol{U}_d$[6] $\boldsymbol{U}_d$[12]	$\boldsymbol{U}_d$[7] $\boldsymbol{U}_d$[13]	$\boldsymbol{U}_d$[8] $\boldsymbol{U}_d$[14]	$\boldsymbol{U}_d$[3] $\boldsymbol{U}_d$[9]
	III	$\boldsymbol{U}_d$[16]	$\boldsymbol{U}_d$[17]	$\boldsymbol{U}_d$[18]	$\boldsymbol{U}_d$[19]	$\boldsymbol{U}_d$[19]	$\boldsymbol{U}_d$[15]
$\left(\frac{-5\pi}{6};\frac{-\pi}{6}\right)$	0	$\boldsymbol{U}_d$[0]	$\boldsymbol{U}_d$[1]	$\boldsymbol{U}_d$[2]	$\boldsymbol{U}_d$[0]	$\boldsymbol{U}_d$[1]	$\boldsymbol{U}_d$[2]
	I	$\boldsymbol{U}_d$[4] $\boldsymbol{U}_d$[10]	$\boldsymbol{U}_d$[5] $\boldsymbol{U}_d$[11]	$\boldsymbol{U}_d$[6] $\boldsymbol{U}_d$[12]	$\boldsymbol{U}_d$[7] $\boldsymbol{U}_d$[13]	$\boldsymbol{U}_d$[8] $\boldsymbol{U}_d$[14]	$\boldsymbol{U}_d$[3] $\boldsymbol{U}_d$[9]
	II	$\boldsymbol{U}_d$[16]	$\boldsymbol{U}_d$[17]	$\boldsymbol{U}_d$[18]	$\boldsymbol{U}_d$[19]	$\boldsymbol{U}_d$[19]	$\boldsymbol{U}_d$[15]
	III	$\boldsymbol{U}_d$[5] $\boldsymbol{U}_d$[11]	$\boldsymbol{U}_d$[6] $\boldsymbol{U}_d$[12]	$\boldsymbol{U}_d$[7] $\boldsymbol{U}_d$[13]	$\boldsymbol{U}_d$[8] $\boldsymbol{U}_d$[14]	$\boldsymbol{U}_d$[3] $\boldsymbol{U}_d$[9]	$\boldsymbol{U}_d$[4] $\boldsymbol{U}_d$[10]
$\left(\frac{\pi}{2},\frac{7\pi}{6}\right)$	0	$\boldsymbol{U}_d$[5] $\boldsymbol{U}_d$[11]	$\boldsymbol{U}_d$[6] $\boldsymbol{U}_d$[12]	$\boldsymbol{U}_d$[7] $\boldsymbol{U}_d$[13]	$\boldsymbol{U}_d$[8] $\boldsymbol{U}_d$[14]	$\boldsymbol{U}_d$[3] $\boldsymbol{U}_d$[9]	$\boldsymbol{U}_d$[4] $\boldsymbol{U}_d$[10]
	I	$\boldsymbol{U}_d$[16]	$\boldsymbol{U}_d$[17]	$\boldsymbol{U}_d$[18]	$\boldsymbol{U}_d$[19]	$\boldsymbol{U}_d$[19]	$\boldsymbol{U}_d$[15]
	II	$\boldsymbol{U}_d$[5] $\boldsymbol{U}_d$[11]	$\boldsymbol{U}_d$[6] $\boldsymbol{U}_d$[12]	$\boldsymbol{U}_d$[7] $\boldsymbol{U}_d$[13]	$\boldsymbol{U}_d$[8] $\boldsymbol{U}_d$[14]	$\boldsymbol{U}_d$[3] $\boldsymbol{U}_d$[9]	$\boldsymbol{U}_d$[4] $\boldsymbol{U}_d$[10]
	III	$\boldsymbol{U}_d$[23]	$\boldsymbol{U}_d$[24]	$\boldsymbol{U}_d$[25]	$\boldsymbol{U}_d$[26]	$\boldsymbol{U}_d$[21]	$\boldsymbol{U}_d$[22]

The choice of inverter voltage vector from the vector voltage selecting table (Table 3) is based on the information on both current N sector, the triangle where voltage vector $\boldsymbol{U}_s^*$ is currently located, as well as the angle of error vector $\varphi_{\varepsilon''}$.

3. Comparison of DTFC3L-3A and DTC methods

The experiments were performed for two values of load i.e. 5 N·m and 10 N·m, and for three set values of angular speed i.e. 50 rad/s, 70 rad/s and 100 rad/s. The motor used in simulations had the following nominal values: $P_n = 4$ kW, $U_n = 400$ V, $f_n = 50$ Hz, $I_n = 8.3$ A, $\omega_n = 150$ rad/s, $\cos\varphi_n = 0.82$. Sample time of control DC/AC converter amounted to 100 μs.

The basis for comparing the methods in the static state were coefficients described by dependencies (16) and (17) [11]. To compare the methods, coefficients of current (17) and torque (16) deformations were determined for each case.

$$M_{(puls)RMS} = \sqrt{\frac{1}{T_o}\int_0^{T_o}(M - M_{AV})^2 dt}, \qquad (16)$$

where $M_{(plus)RMS}$ – RMS value of all of torque harmonics for constant torque set value, T_0 – period of phase current, M – instantaneous value of electromagnetic torque, M_{AV} – mean value of electromagnetic torque.

$$I_{U(puls)RMS} = \sqrt{\frac{1}{T_o}\int_0^{T_o}(i_U - i_{U1})^2 dt}, \qquad (17)$$

where $I_{U(puls)RMS}$ – RMS value of phase current harmonics after subtraction instantaneous value of the first harmonic, i_U – instantaneous value of phase current, i_{U1} – instantaneous value of the first harmonic of phase current.

It should be emphasized here that in order to correctly interpret the simulation results, a three-level inverter was used only in DTFC3L3A method. In such inverters the switchings of switching devices occur at twice lower voltage than in two-level ones. As a result, switching energy losses in three-level inverters operating at the same switching frequency is twice smaller.

The use of the DTFC-3L-3A method made possible to obtain a sinusoidal shape of flux, as well as reduces coefficients of current deformations by current approximately 21–55% compared with the DTC method. It follows from Table 4 that the use of the DTC-3L-3A method increases the number of inverter switchings by 136%. Keeping in mind that all switchings take place at twice lower voltage, switching energy losses, when using this method, should be a higher than with the DTC method by approximately 18%. In the case higher angular frequency, switching energy losses in the DTC-3L-3A method are lower about 36% (for 70 rad/s) and 60.3% (for 100 rad/s) compared with the DTC method.

Table 4
Comparison of current distortions and torque ripples in DTC and DTFC3L3A methods

Method	Set values							
	ω_m^*	rad/s	50		70		100	
	M	N · m	5	10	5	10	5	10
DTC	$I_{U(puls)RMS}$	A	1.028	0.929	0.807	0.829	0.880	0.752
DTFC-3L-3A			0.459	0.483	0.459	0.511	0.595	0.596
DTC	$M_{(puls)RMS}$	N·m	0.775	0.774	0.834	0.785	0.865	0.799
DTFC-3L-3A			0.405	0.409	0.475	0.502	0.476	0.460
DTC	f	kHz	9	9.1	10.6	10.4	10.6	10.7
DTFC-3L-3A			21.3	20.3	13.6	12.9	8.7	8.5

a)

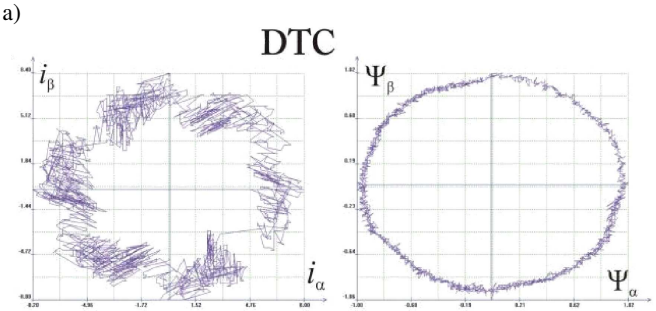

b)

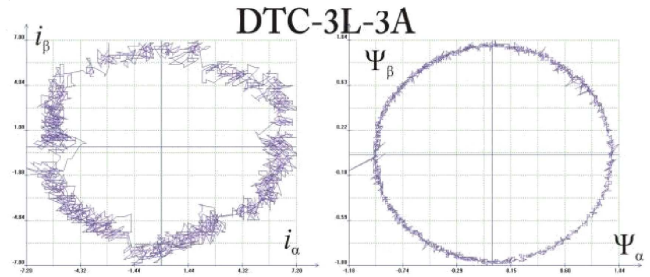

Fig. 13. Hodograph plot of flux and current vectors in $\alpha\beta$ reference frame for set values of angular speed at 50 rad/s and torque 10 N·m for DTC (a) and DTFC-3L-3A (b) methods

4. Conclusions

The results of simulations have shown that using a new modified method of Direct Torque Control is more advantageous. In higher angular frequency, with smaller values of current deformations and torque ripples, it is possible to operate inverters with lower frequency switchings than in DTC methods for the two-level inverter configuration, thus reducing switching energy losses.

Acknowledgements. The work was supported by The National Centre for Research and Development as a scientific project N R01 002406/2009.

REFERENCES

[1] I. Takahashi and T. Noguchi, "A new quick – response and high – efficiency control strategy of an induction motor", *IEEE Trans. on Indust. Appl.* IA-22, 820–827 (1986).

[2] C. Ortega, A. Arias, C. Caruana, J. Balcells, and G.M. Asher, "Improved waveform quality in the direct torque control of matrix-converter-fed PMSM drives", *IEEE Trans. on Indust. Electronics* 57, 2101–2110 (2010).

[3] J. Beerten, J. Verveckken, and J. Driesen, "Predictive direct torque control for flux and torque ripple reduction", *IEEE Trans. on Indust. Electronics* 56, 404–412 (2010).

[4] Kuo-Kai Shyu, Juu-Kuh Lin, Van-Truong Pham, Ming-Ji Yang and Te-Wei Wang, "Global minimum torque ripple design for direct torque control of induction motor drives", *IEEE Trans. on Indust. Electronics* 57, 3148–3156 (2010).

[5] S.A. Zaid, O.A. Mahgoub, and K.A. El-Metwally, "Implementation of a new fast direct torque control algorithm for induction motor drives", *IET Electric Power Applications* 4, 305–313 (2010).

[6] A. Sikorski, M. Korzeniewski, A. Ruszczyk, M.P. Kaźmierkowski, P. Antoniewicz, W. Kolomyjski, and M. Jasiński, "A comparison of properties of direct torque and flux control methods (DTC-SVM,DTC-δ, DTC-2x2, DTFC-3A)", *EUROCON 2007 Int. Conf. on Computer as a Tool* 1, 1733–1739 (2007).

[7] D. Casadei, F. Profumo, G. Serra, and A. Tani, "FOC and DTC: two viable schemes for induction motors torque control", *IEEE Trans. on Indust. Electronics* 17, 779–787 (2002).

[8] H. Benderradji, A. Makouf, and L. Chrifi-Alaoui, "Field-oriented control using sliding mode linearization technique for induction motor", *Control & Automation MED Conf. 18th Mediterranean* 1, 133–1138 (2010).

[9] A. Sikorski, *Direct Control of the Torque and Flux of Induction Motor*, Publishing House of the Białystok University of Technology, Białystok, 2009, (in Polish).

[10] K.Kulikowski and A. Sikorski, "Comparison of new DPC methods for two- and three-level AC/DC converters", *Electrical Review* 87, 56–61 (2011).

[11] M.Korzeniewski and A. Sikorski, "Three-level DC/AC inverter controlled by direct torque and flux control method of induction motor", *Electrical Review* 86, 263–268 (2010).